

Quantized electrical conductivity in binary neutron star mergers

Sreemoyee Sarkar^{1,*} and Souvik Priyam Adhya^{2,†}

¹*Department of Physics, St.Xavier's College-Autonomous, Mumbai - 400001, India.*

²*Institute of Nuclear Physics, Polish Academy of Sciences, Radzikowskiego 152, 31-342 Krakow, Poland*

(Dated: August 27, 2021)

We examine nature of longitudinal electrical conductivity in magnetized electron-ion plasma in the context of binary neutron star mergers. In presence of strong magnetic field, high density and temperature, quantum oscillatory behavior for electrons emerge due to breakdown of the classical description. For pronounced thermodynamic effects, we consider zeroth Landau level population of electrons for electrical conductivity. We solve Boltzmann equation in presence of magnetic field to obtain the dissipative component of the conductivity. The conductivity is formulated considering dynamically scattering centers in the medium with magnetically modified screening. Numerical estimations show that the effect of magnetically modified screening mass on electrical conductivity is less. On the other hand, we observe that frequency dependent screening reduces electrical conductivity leading to a reduction in the Ohmic decay time scale to become of the order of the characteristic timescale of the merger process in the low density regime. This indicates the relevance of dissipative process for the merger simulation in the above mentioned domain.

I. INTRODUCTION

The recent detection of gravitational wave signal GW170817 originating from binary neutron star (BNS) merger by the LIGO and Virgo detectors have opened up a new era in multi-messenger astronomy [1–3]. Additionally, short gamma-ray bursts (SGRBs) were also detected by the Fermi satellite GRB170817A indicating the presence of huge magnetic field in the merging event [4–6]. These mergers are unique astrophysical objects of significant sources of gravitational radiation, electromagnetic as well as neutrino emission [7]. They offer a novel avenue to study highly non-linear gravitational effects blended with complex micro-physical processes; serving as Einstein's richest natural laboratory [8].

In the event post merging, a remnant neutron star is created and if the remnant possess a mass beyond Tolman–Oppenheimer–Volkoff (TOV) limiting mass, the merged object collapses within a few milliseconds. The description of neutron star mergers requires the knowledge of General Relativistic Magneto Hydro-dynamics (GRMHD)[9–17]. Most of these general-relativistic simulations account for ideal Magneto Hydro-dynamics (MHD) limit with infinite electrical conductivity(σ) to arrive at large Ohmic decay time scale. In a recent work [18], the authors have pointed out that Hall decay time scale could be relevant in the survival time period of merged object. In view of these recent studies [18, 19] on the relevance of different transport coefficients in BNS mergers, we analyse the importance of dissipative mechanism in the MHD simulation of mergers by evaluating quantized electrical conductivity with many-body effects and quantify the Ohmic decay time scale.

We consider fully ionized plasma of electrons and ions. Heat and charge in this medium are transported by electrons. The dominant electron transport mechanism is scattering on ions in the liquid phase. In presence of extreme magnetic field ($B \sim 10^{16}G$) and density ($\rho \sim 10^{13}gm/cm^3$), the classical description of electrons breaks down. Therefore, one should incorporate Landau quantization of energy levels in the formalism. This quantization occurs for a particular set of temperature, density and magnetic field in case of neutron star. Thus, the inclusion of Landau quantization eventually modifies the non-magnetic electrical conductivity to great extent[20–23]. In the present paper, we focus mainly on the strongly quantizing case, since in this domain, the transport coefficients receive major modification due to the magnetic field.

The calculation of electrical conductivity by solving Boltzmann equation in ultra-compressed plasma have been studied by several authors over the last few decades [24–28]. This requires the information of scattering rate of plasma constituents. The calculations of scattering rate considering screened Coulomb potential have already been observed in different Refs.[20–23, 29]. In all these calculations it has been assumed that ions are static scatterers. This formulation can not be easily transported to the relativistic domain of large densities where dynamical effects could be important for reliable description of transport coefficients. Medium modified Hard-Thermal-Loop (HTL) and Hard-Dense-Loop (HDL) propagators include dynamical effects in the high temperature and high density plasmas respectively [30–34].

* sreemoyee.sinp@gmail.com

† souvik.adhya@ifj.edu.pl

While Debye screening in plasma is related to the longitudinal photon exchange, the exchange of magnetic/ transverse photons contribute to dynamical screening of the plasma particles. It is observed in different studies [33–40] that for ultra-degenerate case, both in Quantum Chromodynamics (QCD) and Quantum Electrodynamics (QED) plasmas, the transverse interactions not only become important but they dominate over their longitudinal interaction. In a recent calculation [41], the authors have included many-body effects through the HTL modified propagator in the calculation of non-quantized electrical conductivity in a warm neutron star crust. Motivated by all these calculations of inclusion of dynamical screening in different transport coefficients, we include the medium modified propagator in quantized electrical conductivity in the context of BNS merger in the present paper. Here we perform the calculations of σ in an extreme scenario of temperature $\sim 12\text{MeV}$, density $\sim 10^{13}\text{ gm/cm}^3$ and magnetic field $\sim B_{16}G$. Finally, using the strongly quantized electrical conductivity, we estimate the Ohmic decay time scale and compare it with the survival time period of BNS mergers.

The paper is organised as follows. In section II, we present the physical conditions for relativistic and strongly quantized electrons in the BNS merger scenario. Next, in section III we derive the longitudinal electrical conductivity in a dynamically screened QED plasma. We study the Ohmic decay time scale of the magnetic field using the electrical conductivity as the input in section IV. We present numerical results for the electrical conductivity for typical ranges of temperature, magnetic field and density for the ultra-dense plasma along with estimation of Ohmic time scale in section V. Finally, we summarize and discuss the impact of dynamical screening on electrical conductivity and decay times in section VI. In addition, we include the important steps for the derivation of the conductivity in Appendix I.

II. PHYSICAL CONDITIONS

Physical properties of the BNS merger, which forms an unstable configuration are different from isolated neutron stars. We consider simplest possible constituents of post-merger object of electron-ion plasma with fully ionized ions and free mobile electrons in the low density (up to 10^{12} gm/cm^3), high magnetic field regime (up to $10^{17}G$ with $T \sim 15\text{MeV}$). Electron density n_e is related to ion density n_i via $n_e = Zn_i$ where Z is the atomic number of the element. We consider the magnetic field (B) is present along the z direction. Scattering of electrons with ions only contribute in electrical conductivity. In the absence of magnetic field the electron density can be written as,

$$n_e = \frac{2}{(2\pi)^3} \int_0^\infty f(\epsilon) d^3p \quad (2.1)$$

where, $f(\epsilon) = (\exp(\frac{\epsilon-\mu}{kT}) + 1)^{-1}$. μ is the chemical potential written as $\mu^2 = p_f^2 c^2 + m^2 c^4$. In presence of a constant magnetic field, the electronic energy states are obtained as solutions of Dirac equations ([42, 43]). The positive energy states are denoted by quantum numbers ϵ, p_z, p_x, n, s . ϵ is the electron energy, p_z is the electron momentum along the field, $s = \pm 1$ is the helicity, and $n = 0, 1, 2$ enumerates the Landau levels. The energy of the relativistic electrons is given by,

$$\epsilon = \sqrt{p_z^2 c^2 + m^2 c^4 + 2n\hbar\omega_B m c^2}, \quad (2.2)$$

instead of $\epsilon = \sqrt{p_f^2 c^2 + m^2 c^4}$. Here, $\omega_B = ebB_{cr}/(mc^2)$ is the electron cyclotron frequency with $b = B/B_{cr}$ and $B_{cr} = 4.413 \times 10^{13}G$. The ground Landau level is non-degenerate with respect to spin while the higher levels are doubly degenerate. The number density of free electrons in presence of magnetic field is written as,

$$n_e = \frac{m\omega_B}{(2\pi)^2} \int_{-\infty}^{\infty} dp_z \sum_{n,s} f(\epsilon_n) \quad (2.3)$$

The magnetic field strongly quantizes the motion of electrons and different transport coefficients receive significant contribution when the electrons are confined to the zeroth Landau level. We do not consider the situation when ions receive quantum modifications due to the magnetic field. Parameters which determine zeroth level population are as follows [44],

$$\begin{aligned} T_{ce} &= \frac{\hbar\omega_{ce}}{k_B} \approx 1.343 \times 10^8 B_{10^{12}} \text{ K} \\ \rho_B &= 7.045 \times 10^3 \frac{A}{Z} (B_{10^{12}})^{3/2} \text{ g cm}^{-3} \end{aligned} \quad (2.4)$$

B is strongly quantizing if $\rho < \rho_B$ and $T \ll T_{ce}$.

It is convenient to introduce the relativistic parameters $x_r = p_F/m_{ec} \sim 1.008(\frac{\rho_6 Z}{A})^{1/3}$ ($\rho_6 = \rho/10^6$), $T_r = m_e c^2/k_B \sim 5.930 \times 10^9$ K. The electron gas is relativistic for $x_r \gg 1$ or $T \gg T_r$. Hence, if density $\rho > 10^6$ gm cm^{-3} and temperature $T_r > 5.930 \times 10^9$ K, electrons are relativistic corresponding to magnetic field $B = 10^{14}$ G.¹

III. FORMALISM

In the current paper, we consider fully ionized plasma of two components: electrons and positive ions of charge Ze . In case of compact objects, the huge magnetic field quantizes the motion of electrons present in the QED plasma. In this section we derive the expression for electrical conductivity (σ) in presence of strong magnetic field in electron-ion plasma from transport theory. In presence of magnetic field σ is anisotropic and the conductivity tensor is written as,

$$\sigma = \begin{pmatrix} \sigma_{\perp} & \sigma_H & 0 \\ \sigma_H & \sigma_{\perp} & 0 \\ 0 & 0 & \sigma_{\parallel} \end{pmatrix} \quad (3.1)$$

where σ_H is the Hall coefficient. In the above expression, σ_{\parallel} and σ_{\perp} are the parallel and perpendicular components of σ respectively in presence of external magnetic field along z direction. In this section we present the calculation of quantized σ_{\parallel} in electron ion plasma. For the rest of the paper, we re-define σ_{\parallel} as σ .

σ is related to the electric current density (j) and satisfies the constitutive relation $j = \sigma E$ where E is the electric field. We obtain j from kinetic theory and is related to displacement of the electronic distributions from their equilibrium configuration due to the presence of electric field in the plasma. Hence,

$$j = 2e \int \frac{d^3p}{(2\pi)^3} v \Phi \frac{\partial f_0}{\partial \epsilon} \quad (3.2)$$

in the above equation e is the charge of an electron, $v = p/\epsilon$, f_0 is the equilibrium distribution function, p and ϵ are the the energy and the momentum of the particle. In addition, Φ contains the information about the off-equilibrium distribution function which arises due to the presence of electromagnetic field in plasma. The Φ is obtained by solving Boltzmann equation in presence of magnetic field. In presence of small E , the distribution function evolves according to the magnetically modified Boltzmann equation given as [21],

$$\frac{\partial f_{npzs}}{\partial t} + v_z \frac{\partial f_{npzs}}{\partial z} - \dot{\mathbf{p}} \cdot \frac{\partial f_{npzs}}{\partial p_z} = \mathcal{C}[f]. \quad (3.3)$$

In the above equation, f_{npzs} describes the population of electrons defined by the quantum state n, s, p_z . v_z is the z component of the velocity of the particle. The third term in the LHS of eq.(3.3) arises from the Lorentz force term $\dot{\mathbf{p}} = e(\mathbf{E} + \frac{1}{c}\mathbf{v}_p \times \mathbf{B})$. In absence of external magnetic field, the Lorentz force term vanishes. In the Lorentz force, the magnetic field contribution vanishes ($\frac{e}{c}(v_p \times B) \cdot v_p \frac{\partial f_{npzs}}{\partial \epsilon_{n,p_z,s}} = 0$) and we obtain,

$$\dot{\mathbf{p}} \cdot \frac{\partial f_{npzs}}{\partial p_z} \simeq e\mathbf{E} \frac{\partial f_{npzs}}{\partial p_z} \quad (3.4)$$

The RHS of Eq.(3.3) contains the information of scattering rate of electrons with the ions present in the medium,

$$\mathcal{C}[f] = \left. \frac{\partial f_{n,p_z,s}}{\partial t} \right|_{coll} = \sum_f I_{fi}(f_{n'p'_zs'}) \quad (3.5)$$

where, sum is over final state quantum numbers n', p'_z, s' . I_{fi} is the electron-ion scattering rate from initial state (i) to the final state (f) in presence of B . $f_{n'p'_zs'}$ is the distribution function of the scattered state. The distribution function of electrons has two parts in presence of electromagnetic field,

$$f_{n,p_z,s} = f_{n,p_z,s}^0(\epsilon) + \delta f_{n,p_z,s} \quad (3.6)$$

$$f^0(\epsilon) = \frac{1}{\exp([\frac{\epsilon_{n,p_z,s}-\mu}{T}] + 1)} \quad (3.7)$$

¹ We have used $c = k_B = \hbar = 1$, where k_B is the Boltzmann constant and the electric charge e is related to the fine structure constant by $\alpha = e^2/(4\pi) = 1/137$.

where, $f^0(\epsilon)$ and δf are the equilibrium and off- equilibrium distribution functions respectively.

We now proceed to calculate the collision integral considering strongly quantizing magnetic field. To calculate the interaction rate, we consider an electron with momentum $p = (E_p, p_z, p_\perp)$ and mass m exchanges a virtual photon of momentum $q = (q_0, q_z, q_\perp)$ with an in-medium ion of momentum $k = (E_k, k_z, k_\perp)$ and mass M . The electron emerges with momentum $p' = (E_{p'}, p'_z, p'_\perp)$ and ion with momentum $k' = (E_{k'}, k'_z, k'_\perp)$. In order to obtain finite interaction rate, we use the HDL re-summed photon propagator with transverse and longitudinal contributions.

We start with the following expression of the interaction rate [21],

$$I_{fi} = \frac{1}{2E} \int \frac{d^3 p'}{(2\pi)^3 2E'} \int \frac{d^3 k}{(2\pi)^3 2k} \int \frac{d^3 k'}{(2\pi)^3 2k'} [f_{n,p_z,s} g_k (1 - f_{n',p'_z,p'_\perp}) - f_{n',p'_z,p'_\perp} g_{k'} (1 - f_{n,p_z,p_\perp})] (2\pi)^4 \delta^4(p + k - p' - k') |M_{fi}|^2 \quad (3.8)$$

where M_{fi} is the scattering matrix and given as [41],

$$\mathcal{M}_{i \rightarrow f} = -\frac{J_0 J'_0}{q^2 - \Pi_L} + \frac{\mathbf{J}_t \mathbf{J}'_t}{q^2 - \Pi_T} = -\mathcal{M}_L + \mathcal{M}_T, \quad (3.9)$$

where,

$$J^\mu = -e^* \bar{u}(p') \gamma^\mu u(p), \quad (3.10)$$

$$J'^\mu = Z e^* v_k^\mu = Z e^* (1, \vec{k}/M), \quad (3.11)$$

are the components of currents. $e^* = \sqrt{4\pi}e$, Z is the atomic number of the nucleus and v_k is the velocity of ion with momentum k . The Π_T and Π_L HDL photon self-energies are transverse and longitudinal respectively. The form of the electronic spinors are given in the Appendix.

To proceed further, we describe the screening mechanism of electron-ion plasma. In earlier calculations ([24–27]) the authors have implemented static longitudinal component of photon propagator to screen the Coulomb potential,

$$D_{\vec{q}} = \frac{1}{q^2 + m_d^2}, \quad (3.12)$$

. Following linear response theory, for time-dependent electric fields, there exists an additional screening mechanism, along with screened Coulomb potential, related to the energy transfer to the constituents of plasma known as Landau damping. This arises because of non-zero frequency of the plasma. We implement the effects of non-zero frequency in both the electric and magnetic components of the photon propagator computed within the HTL/HDL formalism. In principle in presence of magnetic field the photon propagator should be anisotropic. In the present study we consider the isotropic photon propagator and obtain,

$$D^{\mu\nu}(\omega, \vec{q}) = \frac{P^{\mu\nu}(q)}{q^2 - \Pi_T(q)} + \frac{Q^{\mu\nu}(q)}{q^2 - \Pi_L(q)} \quad (3.13)$$

where $q = (q_0, \vec{q})$ is the four-momentum of the photon and $P_{\mu\nu}$ and $Q_{\mu\nu}$ are the transverse and longitudinal projectors, respectively,

$$P^{ij}(q) = -\delta^{ij} + \frac{q^i q^j}{q^2}, \quad (3.14)$$

$$Q^{00}(q) = -\frac{q^2}{q^2} = 1 - \frac{q_0^2}{q^2} = 1 - y^2. \quad (3.15)$$

The transverse (Π_T) and longitudinal (Π_L) HDL photon self-energies and are given by

$$\begin{aligned} \Pi_T(q) &= 3m_D^2 \left[\frac{y^2}{2} + \frac{y(1-y^2)}{2} \ln \left(\frac{y+1}{y-1} \right) \right] \\ \Pi_L(q) &= 3m_D^2 \left[1 - y^2 - \frac{y(1-y^2)}{2} \ln \left(\frac{y+1}{y-1} \right) \right], \end{aligned} \quad (3.16)$$

where, $m_D^2 = e^2 dn_e/d\mu$.

In presence of strong magnetic field electron density present in the plasma changes, leading to a modification in the screening. At low temperature and strong magnetic field presence of sharp Fermi surface modifies the nature of screening. In the non-relativistic regime where $m \gg \mu$, for large B, the Debye mass is given by

$$m_D^2 = \left(\frac{e}{\pi} \right)^2 \left(\frac{eB}{2} \right) \left(\frac{m}{p_f^z} \right), \quad (3.17)$$

and in the relativistic domain $m \ll \mu$, the Debye mass is given by

$$m_D^2 = \left(\frac{e}{\pi}\right)^2 \left(\frac{eB}{2}\right) \quad (3.18)$$

In order to proceed further, we compute the phase space factor in the interaction rate given in eq.(3.8). We neglect the terms which are quadratic in distribution function as well as we do not consider the change of momentum of ions in the phase space factor. Hence, the phase term can be written as,

$$[f_{n,p_z,s} g_k (1 - f_{n',p'_z,p'_\perp}) - f_{n',p'_z,p'_\perp} g_{k'} (1 - f_{n,p_z,p_\perp})] = g_k (f_{n,p_z,p_\perp} - f_{n',p'_z,p'_\perp}) \quad (3.19)$$

Thus the final expression for the interaction rate is obtained as (details in Appendix),

$$I_{fi} = \frac{n_i}{2} \sum_n \int du (f_{n,p_z,p_\perp} - f_{n',p'_z,p'_\perp}) \left[\frac{1}{3(u + \frac{\xi}{3})(u + \xi)} - \frac{v_k^2}{6u(u + \frac{\xi}{3})} \right] \mathcal{F} \quad (3.20)$$

where, n_i is the number density of ions. In order to find the transport coefficients, it is useful to define a dimensionless scattering rate a and a dimensionless perturbation to the distribution function (f_1) defined as,

$$\begin{aligned} \frac{I_{fi}}{n_i v_z \sigma_0} &= a \\ \frac{eE}{\sigma_0 n_i} \frac{\partial f_0}{\partial \epsilon} \Phi &= f_1 \end{aligned} \quad (3.21)$$

where, $\sigma_0 = \pi Z^2 e^4 / \omega_B^2$, $\omega_B = eB / m_e c$. Using the above two equations, we obtain the dimensionless form of the linearized Boltzmann equation as shown below [45],

$$\sum_{n' s' \gamma} a(ns \rightarrow n' s') (\Phi_{n' s'} - \gamma \Phi_{ns}) = 1. \quad (3.22)$$

$\gamma = \pm$ denotes the scattering channel for forward (+) and backward reactions (-). In the current paper, we present the results for the strongly quantizing scenario (i.e. zeroth Landau level) which provides the maximum effect with finite magnetic field in contrast to the non-magnetic scenario. For zeroth Landau level, $n = n' = 0$, spin degeneracy is absent and backward scattering ($\gamma = -1$) is the only allowed channel for scattering. Hence, after solving the dimensionless Boltzmann equation the off equilibrium distribution function is obtained as,

$$\Phi = \frac{E^2 - 1}{2Q_2} \quad (3.23)$$

where, $E = \epsilon / mc^2$, $\Phi \equiv \Phi_{0,-1}$ and

$$Q_2 = \int_0^\infty e^{-u} \left[\frac{2}{3(u + \frac{\xi}{3})(u + \xi)} - \frac{v_k^2}{6u(u + \frac{\xi}{3})} \right] du \quad (3.24)$$

Finally, we obtain the expression for electrical conductivity for zeroth Landau level by inserting the value of Φ in the equation below,

$$j_z = \frac{em\omega_B}{4\pi^2} \int_{mc^2}^\infty f_1 d\epsilon \quad (3.25)$$

and then comparing with $j_z = \sigma E$. Thus the final form of σ becomes,

$$\sigma = \frac{m^4 b^2}{8\pi^3 Z^2 e^2 n_i} \int_{mc^2}^\infty \frac{\partial f_0}{\partial \epsilon} \Phi d\epsilon \quad (3.26)$$

The above expression can be written in more compact form by introducing energy dependent electron relaxation time $\tau(\epsilon)$,

$$\sigma = e^2 \int_{mc^2}^\infty \frac{\mathcal{N}(\epsilon) \tau(\epsilon)}{\epsilon} \left(-\frac{\partial f}{\partial \epsilon} \right) d\epsilon \quad (3.27)$$

where, $\tau(\epsilon)$ is

$$\begin{aligned} \tau(\epsilon) &= \frac{\epsilon l m \omega_B \Phi}{2\pi^2 \mathcal{N}(\epsilon)} \\ \mathcal{N}(\epsilon) &= \frac{2m\omega_B}{4\pi^2} p_{n=0}(\epsilon) \end{aligned} \quad (3.28)$$

l is the electron scattering length $l = \frac{mc^2 \omega_B}{2\pi n_i Z^2 e^4}$.

IV. OHMIC DECAY TIME SCALE

The estimation of Ohmic dissipation time scale is important to assess the limit of the ideal MHD approximation. Ideal MHD is defined to be the limit in which the electrical resistivity $\eta = 1/\sigma$ vanishes. Using Maxwell's equation one can obtain the magnetic field decay time scale as described below. We start with Ampere's and Faraday's law,

$$\begin{aligned}\vec{\nabla} \times \vec{B} &= \frac{4\pi\vec{j}}{c} \\ \vec{\nabla} \times \vec{E} &= -\frac{\partial\vec{B}}{\partial t}.\end{aligned}\tag{4.1}$$

Now, $j = \sigma E$ and resistivity $\rho = c^2/4\pi\sigma^{-1}$. Using these two in the above Eq.(4.1) Ohm's law can be written as follows by eliminating electric field.

$$\frac{\partial\vec{B}}{\partial t} = -\vec{\nabla} \times \left(\frac{c}{4\pi\sigma} \vec{\nabla} \times \vec{B} \right).\tag{4.2}$$

The above equation is termed as the induction equation. Using vector identity $\vec{\nabla} \times (\vec{\nabla} \times \vec{B}) = \vec{\nabla} (\vec{\nabla} \cdot \vec{B}) - \nabla^2 \vec{B}$ and $\vec{\nabla} \cdot \vec{B} = 0$, we obtain from Eq. (4.1),

$$\frac{4\pi\sigma}{c^2} \frac{\partial\vec{B}}{\partial t} = \nabla^2 \vec{B}.\tag{4.3}$$

A qualitative estimate of the magnetic field decay timescale (τ) can be obtained from Eq. (4.3) if we approximate $|\nabla^2 \vec{B}| \simeq B/\lambda_B^2$ and $|\partial\vec{B}/\partial t| \simeq B/\tau$, where, λ_B^2 is the characteristic length scale of variation of the magnetic field. From these estimates, we find that the magnetic field decay (or diffusion) timescale due to Ohmic dissipation is given by the well-known expression [46, 47],

$$\tau = \frac{4\pi\sigma\lambda_B^2}{c^2}.\tag{4.4}$$

In the next section, we study the effects of the frequency dependent screening on τ entering through the σ as defined in the above equation.

V. RESULTS AND DISCUSSIONS

In this section we describe the behaviour of longitudinal quantized electrical conductivity with density, temperature, magnetic field and atomic number for the hot and dense electron-ion plasma. In the merger scenario, the electrons are considered relativistic for $T_{tr} > 5 \times 10^9$ K and density $\rho \sim 10^6$ gm cm^{-3} . The momentum of an electron is related to the energy via the relation $p_{nz}/(mc^2) = \sqrt{(\epsilon/mc^2)^2 - 2bn - 1}$. From this expression one can obtain the maximum Landau level that the electrons can populate and is given by the integer part of $\nu = (E^2 - 1)/2b$ ($E = \epsilon/mc^2$). The energy of the electrons is constrained to $(E^2 - 2b) < 1$ to meet the condition of lowest Landau level. This is an important condition to be used to obtain the desired results for the plots of σ as we describe later in this section. The parameters for density, temperature and magnetic field are appropriately chosen for relativistic quantized electrons to simultaneously meet the physical conditions applicable for the merging scenario.

A. Variation with atomic number

In fig.1, we have plotted σ with ρ for two different equation of states (EOS): BPS (Baym, Pethick and Surtherland) [48] and magnetic BPS model [49]. In ref.[48] the equation of state of zero-temperature matter in complete nuclear equilibrium is given for mass densities below 5×10^{14} g cm^{-3} . In Ref.([49]), the BPS [48] has been extended to include the physical parameters for a low density plasma in presence of high magnetic field relevant for neutron star crust. We choose *Mo* for calculations of σ at higher density as shown in fig.1. In addition, we have also presented results for *Fe* as a reference. Thus, we consider these two elements for the estimation of σ .

B. Effect of magnetically modified electronic screening

In the figs.2(a) and 2(b) we have shown the variation of σ with density for *Mo* and *Fe* respectively. For the current plot we consider magnetically modified static screened Coulomb potential. We consider two different sets of temperature. It can be seen that the effect of screening is negligible in electrical conductivity. Next we introduce the medium modifications through the HDL corrected photon propagator for the calculation of σ .

C. Effect of HDL modified propagator

We have plotted σ with ρ in Fig.3(a) and Fig.3(b) for different temperatures and at a fixed magnetic field with the HDL modifications through the interaction rate. We find that the inclusion of HDL propagator in the calculation reduces the value of σ substantially.

It is known that modifications to different equilibrium and non- equilibrium properties of plasma due to inclusion of HDL propagators emerge from frequency dependent transverse component of the propagator. However in case of σ , inclusion of the transverse photon does not provide a significant change as the transverse term contains a pre- factor which is inversely proportional to the mass of the ions. The reduction in σ arises due to increase of the interaction rate caused by non- zero component of the plasma frequency.

D. Variation with density

Figs.4 shows the variation of σ with ρ for different temperatures and at fixed magnetic fields. In order to consider electrons to be relativistic, the density and temperatures are chosen as $\rho \gg 10^6 \text{ gm/cm}^3$ and $T \gg T_r$ respectively. For fixed B , μ increases with ρ and electrons start to populate higher Landau levels. Since, we are interested in population of the zeroth Landau level, the density and temperature should satisfy $\rho < \rho_B$ and $T \ll T_{ce}$ as defined in Eq.(2.4). With all these conditions, σ has been obtained by numerically integrating the expression Eq.(3.26). The variation of σ with ρ in the fig. (4) shows that at temperature $\leq 10^{10}$ K, a prominent hump is present. This nature occurs because at this density the weak degeneracy condition ($|\epsilon - \mu| \sim T$) of electron distribution function is fulfilled. The nature of the curve resembles differentiated Fermi function at $T \ll \mu$. As the temperature increases, the hump gets flattened since electrons start becoming non-degenerate.

E. Variation with temperature and magnetic field

Fig.(5) shows variation of σ with T for different densities. The plot shows hump at particular temperature where the density is such that the condition $(e - \mu) \sim T$ is satisfied. The σ in fig.(5) can be fitted as,

$$\begin{aligned} \sigma &= (a + b \times T^c)^{-1} \\ a &= 1.45 \times 10^{-25} \\ b &= 1.05 \times 10^{-46} \\ c &= 1.919 \end{aligned} \tag{5.1}$$

At low temperature the effect of T^c is very small, hence, σ is constant. On the other hand at high temperature $\sigma \propto T^{-c}$ and decreases with temperature. Thus, at higher temperatures, the electrons become classical obeying the inverse dependence of temperature. Fig.(6) shows the variation of σ with magnetic field B for different densities. The fitting parameters for the σ with B is obtained as,

$$\begin{aligned} \sigma &= A_0 + A_1 B + A_2 B^2 \\ A_0 &= 5.15 \times 10^{27} \\ A_1 &= -2.71 \times 10^{11} \\ A_2 &= 5.30 \times 10^{-6} \end{aligned} \tag{5.2}$$

The peak in the left panel occurs at $\epsilon - \mu(B) \sim T$. On increasing the magnetic field, σ increases with B and saturates. For higher temperature (right panel), σ shows a gradual increment with B .

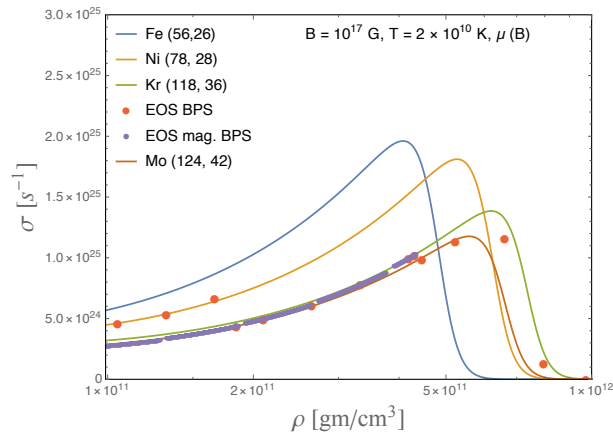


FIG. 1: The comparison of σ with ρ for different elements. The magnetic field is chosen as $10^{17}G$ and temperature as $2 \times 10^{10}K$. We have shown the comparison with the EOS [48, 49]

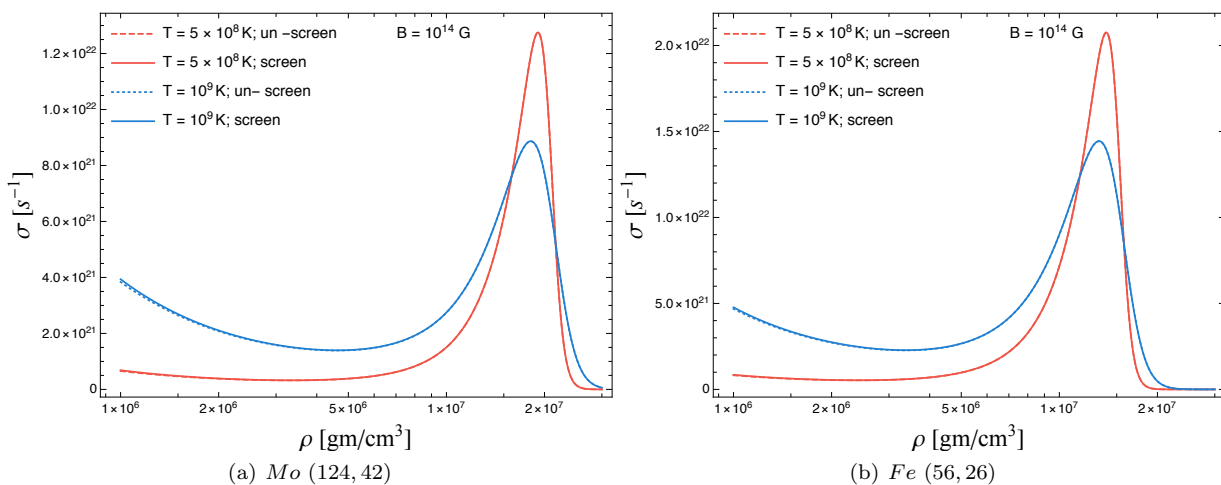


FIG. 2: The comparison of σ with ρ for magnetically modified Debye screening and non-magnetic Debye screening cases for different values of temperature at a fixed field of $10^{14}G$. The choice of elements are *Mo* (124, 42) (left panel) and *Fe* (56, 26) (right panel) respectively.

F. Estimation of Ohmic time scale

The decay timescale of magnetic field due to the Ohmic dissipation is given by the expression Eq.(4.3). For the estimation of the time scale, the information of average scale height of magnetic field is required. The average scale is defined as $\lambda_B \equiv B/\nabla B$ and a limiting value has been assigned to it following $\lambda_B \simeq 0.1 \times 10^{-5} (T/1MeV)^{-1/2} m$ [18], In fig.7, we present the estimation of the Ohmic decay timescale for a typical range of density and temperature for two values of the magnetic field. We find the timescale $\sim 1 - 2 ms$ which is well within the range of survival time period of neutron star merger. However, the naive estimation presented here demands a more realistic and detailed derivation of different time scales to assess the validity of MHD simulation in neutron star mergers.

VI. SUMMARY AND CONCLUSIONS

In this work, we have calculated the quantized longitudinal electrical conductivity in presence of magnetic field followed by numerical results which account for the inclusion of the dynamical screening in the calculation. The calculation has been performed considering electron-ion plasma where the dominant mechanism is the scattering of electrons with ions through screened electromagnetic force. We have presented the plots of variation of electrical

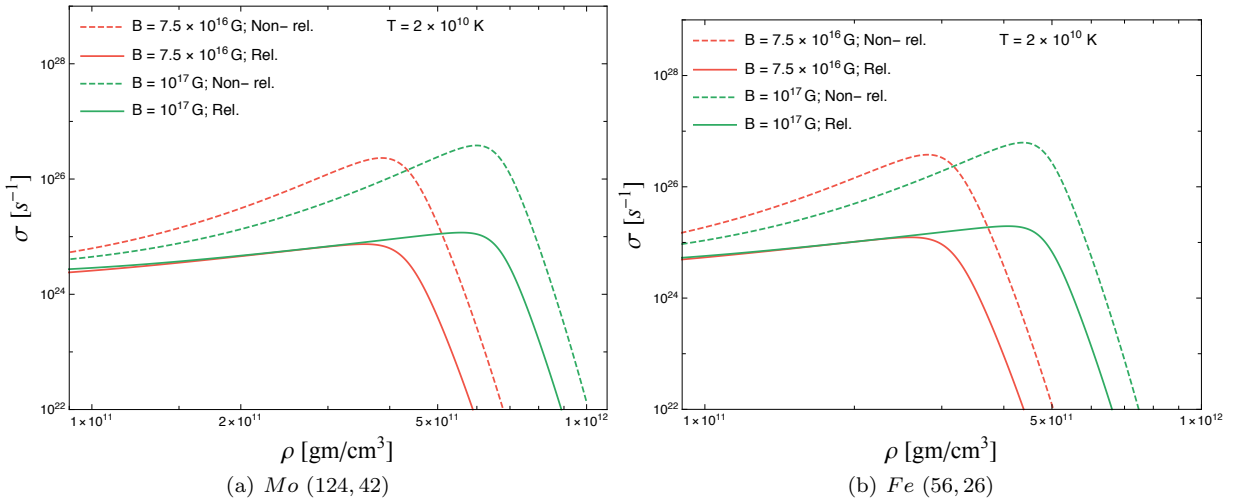


FIG. 3: The comparison of σ with ρ considering relativistic and non-relativistic photon polarisation functions for different values of magnetic field at a fixed temperature of 2×10^{10} K. The choice of elements are *Mo* (124, 42) (left panel) and *Fe* (56, 26) (right panel) respectively.

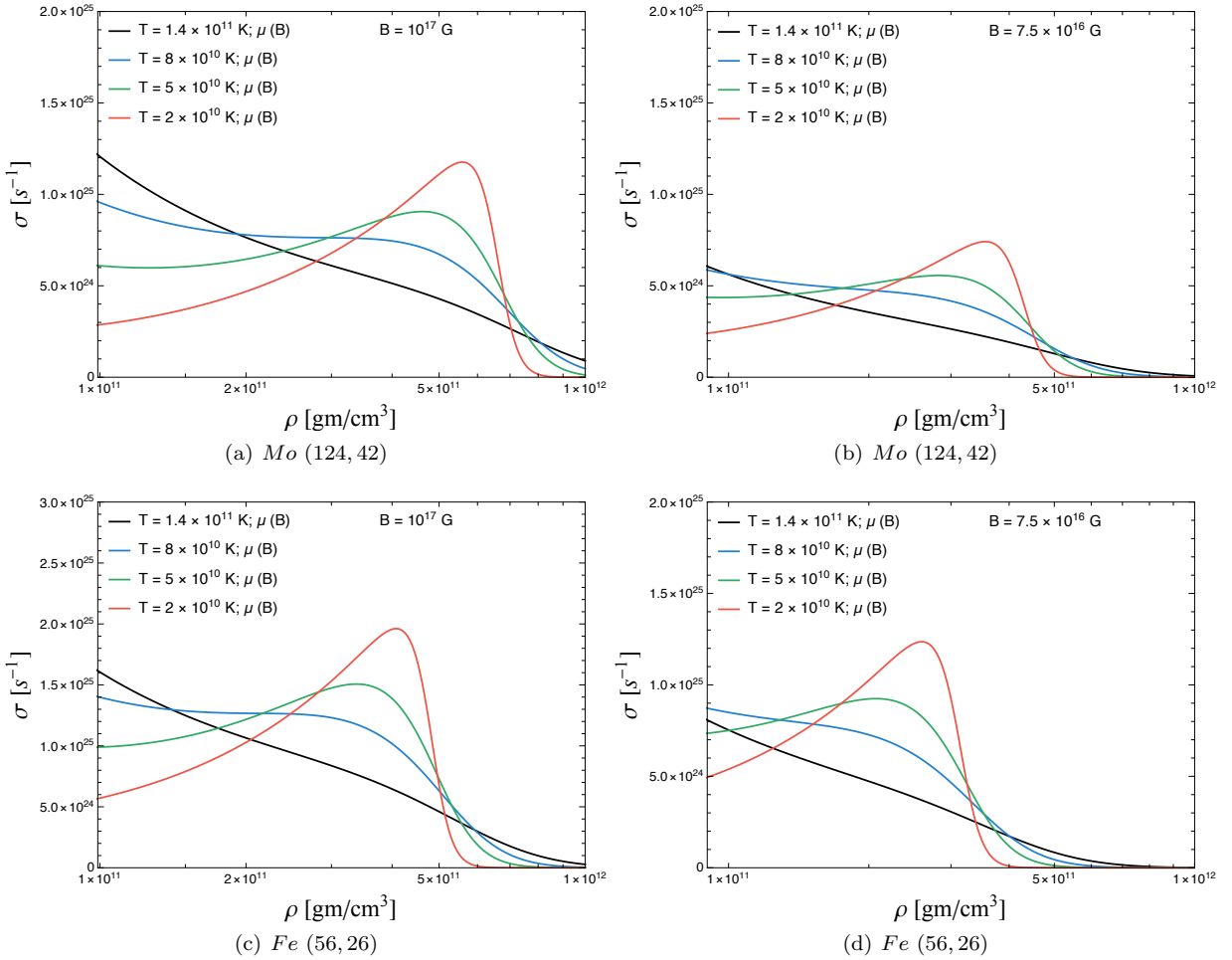


FIG. 4: The comparison of σ with ρ for different values of temperature. The magnetic fields chosen are 10^{17} G (left panel) and 7.5×10^{16} G (right panel) respectively. The choice of elements are *Mo* (124, 42) (upper panel) and *Fe* (56, 26) (lower panel) respectively.

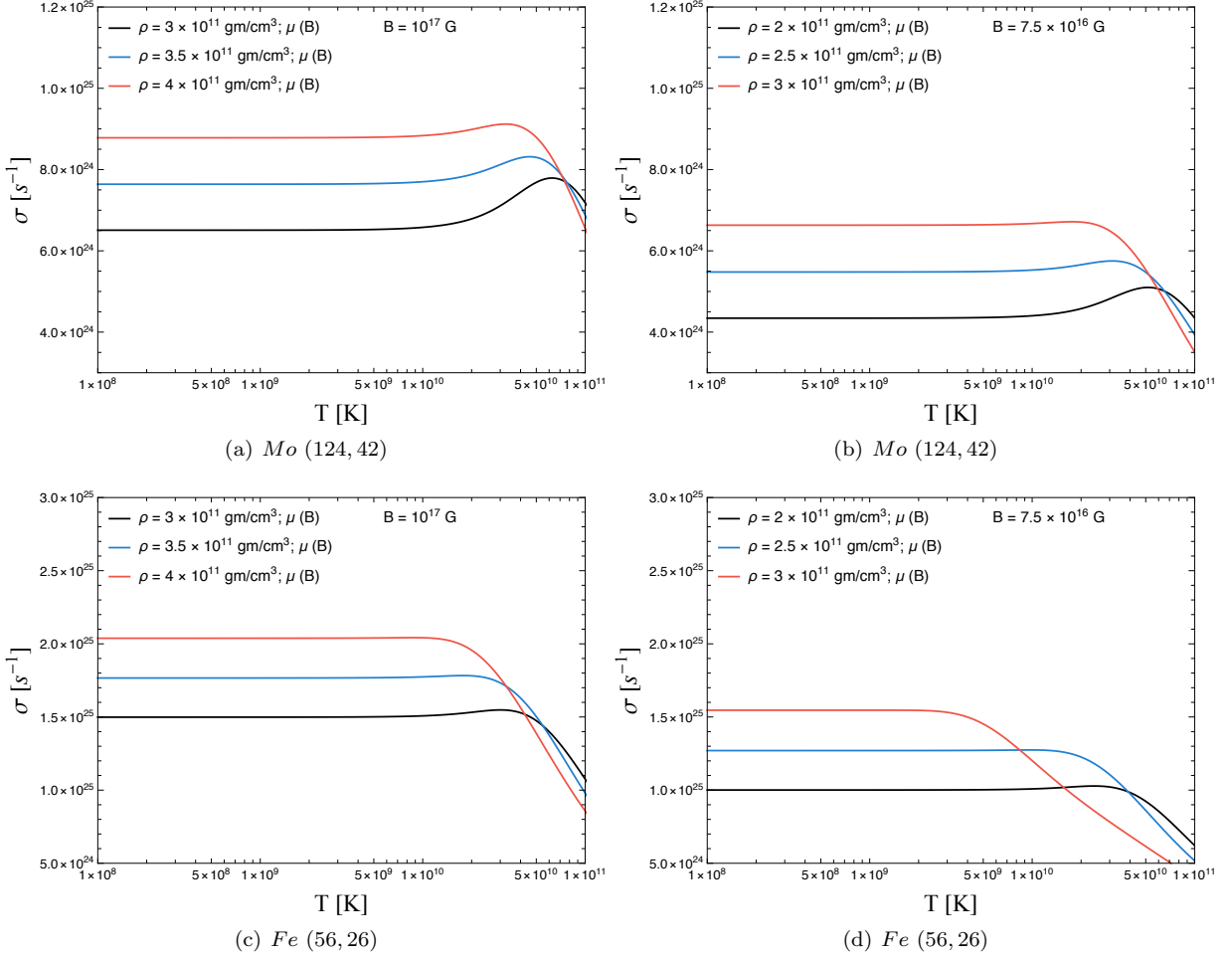


FIG. 5: The comparison of σ with T for different values of magnetic field. The fields chosen are $10^{17}G$ (left panel) and $7.5 \times 10^{16}G$ (right panel) respectively. The choice of elements are *Mo* (124, 42) (upper panel) and *Fe* (56, 26) (lower panel) respectively.

conductivity with density ($\sim 10^{12} \text{ gm/cm}^3$), temperature ($\sim 10^{10} \text{ K}$) and magnetic field ($\sim 10^{17} \text{ G}$) considering two metals *Mo* and *Fe*. The scales for the generation of the plots are chosen so that they obey primarily the conditions that the electrons become relativistic at density $\rho > 10^6 \text{ gm/cm}^3$ and temperature $T > 5.93 \times 10^9 \text{ K}$ and electrons remain confined to zeroth Landau level by obeying the condition $\sqrt{E^2 - 1}/2b \ll 1$. Considering these two constraints, the domain of validity of our calculations lie in the high magnetic field and low density plasma of BNS mergers.

For the calculation of conductivity, we have assumed particles are slightly out of equilibrium which allows us to solve the Boltzmann equation numerically. We have considered electron-ion scattering amplitude via screened electromagnetic interaction using magnetically modified spinors. The off-equilibrium distribution function has been obtained by solving the Boltzmann kinetic equation in relaxation time approximation. However, we have not considered the finite size of the nuclei and ion structure function for the calculation of the relaxation rate.

The electromagnetic interaction between electrons and ions have been incorporated through HDL propagators in the calculation. The calculation should account for magnetically modified anisotropic photon propagator; however for the present paper, we have considered only isotropic HDL propagator and aim to include magnetically modified propagator in an upcoming work [50]. We have observed that the effect of magnetically modified Debye screening is negligible in electrical conductivity.

We have found that the inclusion of the HDL propagator reduces the value of σ in contrast to static screening. The transverse component of the propagator contributes less to the conductivity since it is inversely proportional to the mass of the ion. The frequency dependent screening in the longitudinal component of the HDL propagator enhances the interaction rate thereby causing a decrease in σ . Next, we have estimated the Ohmic decay time scale from the expression of quantized σ including frequency dependent screening. The obtained time scale is of the same order

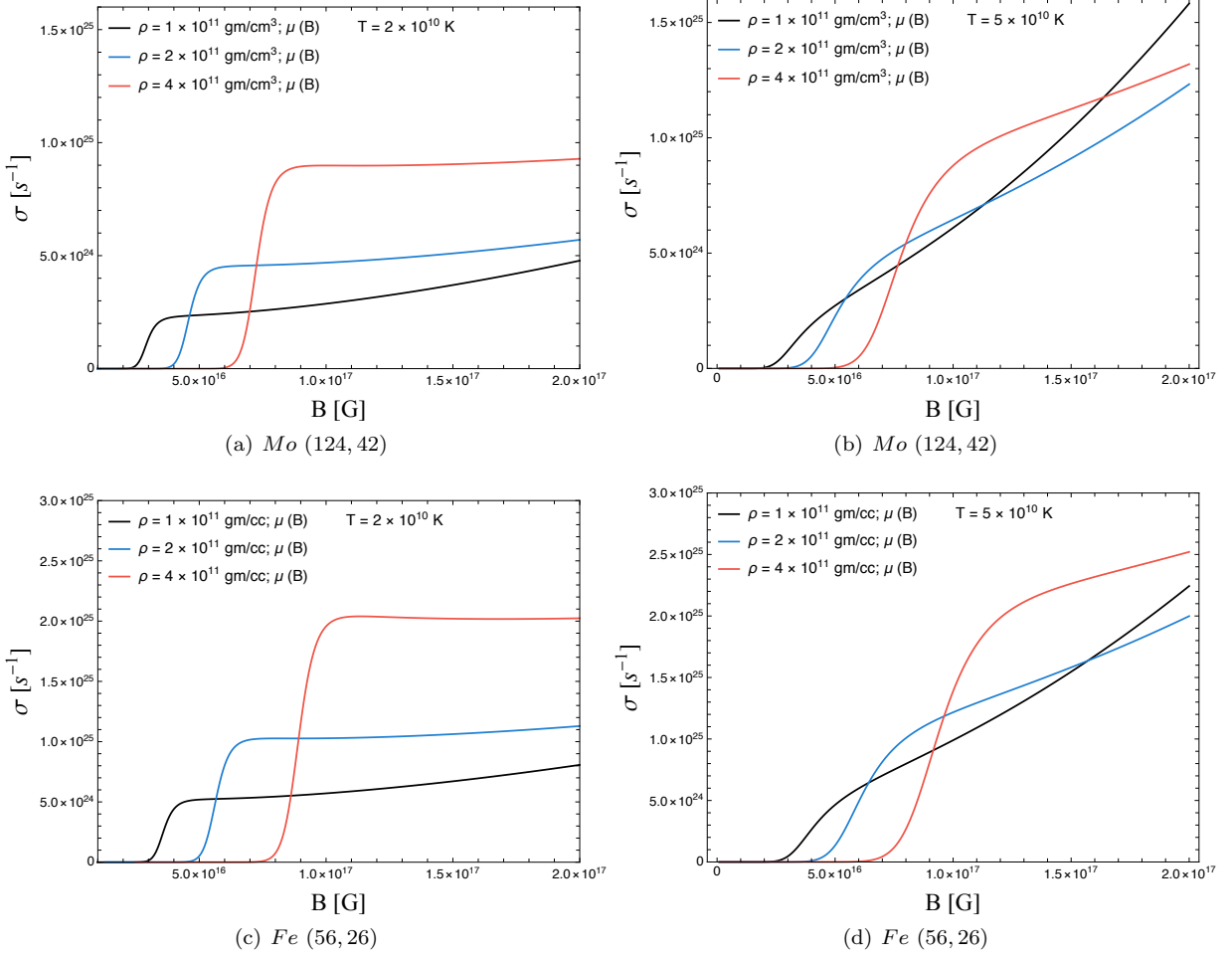


FIG. 6: The comparison of σ with B for different values of density. The temperatures chosen are $2 \times 10^{10}K$ (left panel) and $5 \times 10^{10}K$ (right panel) respectively. The choice of elements are Mo (124, 42) (upper panel) and Fe (56, 26) (lower panel) respectively.

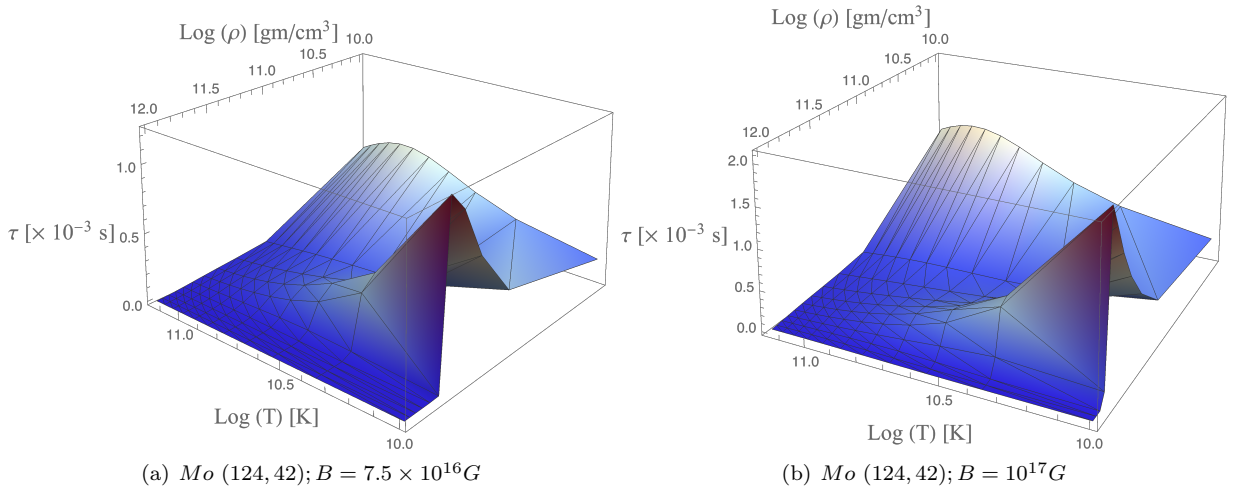


FIG. 7: The estimation of τ with ρ and T . The magnetic field is chosen as $10^{17}G$ and $7.5 \times 10^{16}G$ respectively for Mo (124, 42).

as the survival time of the merged compact object. Hence, one can infer that many-body effects play an important role in determining the dissipative time scales relevant in the neutron star merger. In the current paper, we have considered only longitudinal electrical conductivity (and ignored all the other tensorial components) in the equation for magnetic-field evolution in plasma. Hence, the realistic estimate of τ can only be obtained if all the components of conductivity tensor are known in the background of relevant equation of state for neutron star merger. However, our calculations presented in this paper provide a significant step towards conjoining the many body effects in plasma with observational hydrodynamic simulations.

Acknowledgments

SS would like to thank DST- INSPIRE faculty scheme Award no.: DST/INSPIRE/04/2015/002594 during the tenure of which this work was initiated and UM-DAE CEBS for hosting the INSPIRE project. Authors would also like to thank and acknowledge Rana Nandi for providing the EOS data as well as fruitful discussions regarding various aspects of this work. Authors acknowledges fruitful discussion with Tanay Mazumdar regarding numerical analysis of the current project. SPA would like to acknowledge IPNP, Charles University, Prague where the initial stages of the work was carried out.

APPENDIX I

In this Appendix, we present the important steps for the evaluation of electron-ion scattering rate in presence of magnetic field. An electron of momentum $P(\epsilon_p, \vec{p})$ scatters with an ion of momentum $K(\epsilon_k, \vec{k})$ leading to the final momentum states $P'(\epsilon_{p'}, \vec{p}')$ and $K'(\epsilon_{k'}, \vec{k}')$. The scattering rate from initial state to final state is given by,

$$I_{fi} = \frac{1}{4} \int \frac{d^3 p'}{(2\pi)^3 2} \int \frac{d^3 k}{(2\pi)^3 2} \frac{d^3 k'}{(2\pi)^3 2} [n_f(p)g_f(k)(1 - n_f(p')) - n_f(p')g_f(k')(1 - n_f(p))] (2\pi)\delta(\epsilon_p + \epsilon_k - \epsilon_{p'} - \epsilon_{k'})\delta^3(\vec{p} + \vec{k} - \vec{p}' - \vec{k}')|\mathcal{M}_{fi}|^2 \quad (6.1)$$

The above equation can be modified in presence of non-zero magnetic field as,

$$I_{fi} = \frac{eB}{(2\pi)^2} \sum_n \int dp'_z dy_B \frac{d^3 k}{(2\pi)^3} \frac{dq_y}{16} \int \frac{d\Omega_k}{4\pi} g_f(k)[n_f(p) - n_f(p')]\delta(\epsilon_p + \epsilon_k - \epsilon'_p - \epsilon'_k) \sum_{q_x, q_z} \delta_{k'_x - k_x, q_x} \delta_{k'_z - k_z, q_z} |\mathcal{M}_{fi}|^2 \quad (6.2)$$

where, $y_B = \frac{p_x}{m\omega_B}$ and we have inserted $\int d\Omega_k/4\pi = 1$. The argument of delta function can be written as follows,

$$\delta(\epsilon_p + \epsilon_k - \epsilon_{p'} - \epsilon_{k'}) = \delta(\epsilon_k - \epsilon_{k'} - \hat{p} \cdot \vec{q}) \quad (6.3)$$

where, we have used $\epsilon_{|p'|} = \epsilon_{|p-q|} = \epsilon_p - \hat{p} \cdot \vec{q}$. The angular integrals of \vec{k} can be expressed as,

$$\int \frac{d\Omega_k}{4\pi} \delta(\hat{p} \cdot \mathbf{q} - v_k \cdot \mathbf{q}) = \frac{1}{2q} \int \frac{d\Omega_k}{4\pi} \delta(\hat{p} \cdot \mathbf{q} - v_k \cdot \mathbf{q}) (\hat{p} \cdot \hat{k} - \hat{p} \cdot \hat{q} \hat{q} \cdot \hat{k})^2 = \frac{1}{4q} \left(1 - \frac{(\hat{p} \cdot \mathbf{q})^2}{q^2}\right) \left((v_k^2 - \frac{(\hat{p} \cdot \mathbf{q})^2}{q^2})\right) \quad (6.4)$$

Eq.(6.2) can be written as,

$$I_{fi} = \frac{n_i}{(2\pi)^2} \sum_n \int dq_z dq_x \frac{dq_y}{16 \times 2q} g_f(k)[n_f(p) - n_f(p')]\mathcal{M}_{fi}|^2 \quad (6.5)$$

where, we have changed the variable $dy'_B = \hbar dq_x/m\omega_B$ following momentum conservation $p'_x - p_x = q_x$. In the above equation, n_i is the number density of ions which can be expressed in terms of electron number density as $n_i = n_e/Z$. Further, n_e can be expressed in terms of the Debye mass as $n_e = \mu m_D^2/3e^2$, where, $m_D^2 = e^2 \mu^2/\pi^2$.

Next we introduce a dimensionless variable $y = q_z/q$,

$$I_{fi} = \frac{\mu m_D^2 eB}{3Ze^2(2\pi)^2} \int dy dq_x \frac{dq_y}{16 \times 2} (n_f(p) - n_f(p'))|\mathcal{M}_{fi}|^2$$

In order to calculate $|\mathcal{M}|^2$, we use following electronic spinor in presence of magnetic field,

$$u(p) = \begin{pmatrix} \tilde{\alpha} \tilde{A} H_{n-1}(\xi) \\ -s \tilde{\alpha} \tilde{\beta} \tilde{H}_n(\xi) \\ s \tilde{\beta} \tilde{A} \tilde{H}_{n-1}(\xi) \\ \tilde{\beta} \tilde{B} \tilde{H}_n(\xi) \end{pmatrix}. \quad (6.6)$$

Using above spinors and the expression for photon propagator(Eq.(3.16)) in Eq.(6.7) one obtains,

$$\sum_{spin} |\mathcal{M}|^2 = (4\pi Z e^2)^2 \left[\frac{2\pi y m_D^2}{(q_\perp^2 + \text{Re}\Pi_L)^2 + \text{Im}\Pi_L^2} - \frac{2\pi y m_D^2 v_f^2}{2(q_\perp^2 + \text{Re}\Pi_T)^2 + \text{Im}\Pi_T^2} \right] [ss' \tilde{\alpha}^2 + \tilde{\beta}^2] [ss' \tilde{A} \tilde{A}' I_{n'-1} I_{n-1}(q_\perp) + \tilde{A} \tilde{A}' I_{n'-1} I_{n-1}(q_\perp)]^2, \quad (6.7)$$

where, s and s' are \pm ,

$$\begin{pmatrix} \tilde{\alpha} \\ \tilde{\beta} \end{pmatrix} = \begin{pmatrix} \sqrt{\frac{1}{2}(1 + \frac{mc^2}{\epsilon})} \\ \sqrt{\frac{1}{2}(1 - \frac{mc^2}{\epsilon})} \end{pmatrix}, \quad (6.8)$$

$$\begin{pmatrix} \tilde{A} \\ \tilde{B} \end{pmatrix} = \begin{pmatrix} \left[\frac{1}{2} \left(1 + \frac{sp_z c}{\sqrt{\epsilon^2 - m^2 c^4}} \right) \right]^{1/2} \\ \left[\frac{1}{2} \left(1 - \frac{p_z c}{\sqrt{\epsilon^2 - m^2 c^4}} \right) \right]^{1/2} \end{pmatrix} \quad (6.9)$$

and

$$I_{n',n} = \int_{-\infty}^{\infty} \exp(iq_y y) \tilde{H}_{n'}(\xi') \tilde{H}_n(\xi) dy, \quad (6.10)$$

$$H_n(\xi) = \frac{m\omega_B}{\pi\hbar} \frac{1}{4} (2^n n!)^{-\frac{1}{2}} \exp\left(-\frac{\xi^2}{2}\right) H_n(\xi) \quad (6.11)$$

$H_n(\xi)$ is the Hermite polynomial, $\xi = \sqrt{m\omega_B}$. Inserting above expressions in Eq.(6.9) we obtain,

$$\sum_{spin} |\mathcal{M}|^2 = (4\pi Z e^2)^2 \left[\frac{2\pi y m_D^2}{(q_\perp^2 + \text{Re}\Pi_L)^2 + \text{Im}\Pi_L^2} - \frac{2\pi y m_D^2 v_f^2}{2(q_\perp^2 + \text{Re}\Pi_T)^2 + \text{Im}\Pi_T^2} \right] \left[1 + ss' + \frac{m^2 c^4}{\epsilon^2} (1 - ss') \left[1 + ss' - \frac{1}{2} \frac{ss' c^2}{\epsilon^2 - m^2 c^4} (\eta' p_{n'} - p_z)^2 \right] [F_{n',n}^2(q_\perp) + F_{n'-1,n-1}^2(q_\perp)] \right] - \frac{ss' u \hbar \omega_B m c^2}{\epsilon^2 - m^2 c^4} [F_{n'-1,n}^2(q_\perp) + F_{n',n-1}^2(q_\perp)] - \frac{sp_z c + s' \eta' p_n' c}{\sqrt{\epsilon^2 - m^2 c^4}} [F_{n',n}^2(q_\perp) - F_{n'-1,n-1}^2(q_\perp)] \quad (6.12)$$

where, $\eta' = \pm$, $F_{n',n} = \exp^{-u/2} u^{\frac{n-n'}{2}} \sqrt{\frac{n!}{n'}} L_{n'-n'}^{n-n'}$ and $u = \frac{1}{2m\omega_B} (q_x^2 + q_y^2)$. The functions $L_{n'-n'}^{n-n'}(u)$ are Laguerre polynomials and $F_{n',n}(u)$ are normalized as $\int_0^\infty F_{n',n}^2 du = 1$.

Now, to perform the integration in y in Eq.(6.6) we use the following sum rule,

$$\int_{-1}^1 \frac{dy}{y} \frac{1}{2\pi} \frac{2 \text{Im} \Pi_L(y)}{(\mathbf{q}^2 + \text{Re} \Pi_L(y))^2 + (\text{Im} \Pi_L(y))^2} - \frac{2 \text{Im} \Pi_T(y)}{(\mathbf{q}^2 + \text{Re} \Pi_T(y))^2 + (\text{Im} \Pi_T(y))^2} = \left(\frac{1}{\mathbf{q}^2 + \text{Re} \Pi_{T,L}(y=\infty)} - \frac{1}{\mathbf{q}^2 + \text{Re} \Pi_{T,L}(y=0)} \right) \quad (6.13)$$

In the limiting case, $\text{Re} \Pi_{T,L}(y=\infty) = \frac{m_D^2}{3}$, $\text{Re} \Pi_T(y=0) = 0$, $\text{Re} \Pi_L(y=0) = m_D^2$.

Using the above relations the interaction rate becomes,

$$I_{fi} = \frac{n_i}{(2\pi)^2} \int dq_x \frac{dq_y}{16 \times 2} (n_f(p) - n_f(p')) \left[\frac{2}{3(q_\perp^2 + \frac{m_D^2}{3})(q_\perp^2 + m_D^2)} - \frac{v_f^2}{6q_\perp^2 (q_\perp^2 + \frac{\mu^2}{3})} \right] \mathcal{F}, \quad (6.14)$$

where,

$$\begin{aligned} \mathcal{F} = & \frac{4\pi\sigma_0}{m^2} [1 + ss' + \frac{m^2 c^4}{\epsilon^2} (1 - ss') [1 + ss' - \frac{1}{2} \frac{ss' c^2}{\epsilon^2 - m^2 c^4} (\eta' p_{n'} - p_z)^2] [F_{n',n}^2(u) + F_{n'-1,n-1}^2(u)]] \\ & - \frac{ss' u \hbar \omega_B m c^2}{\epsilon^2 - m^2 c^4} [F_{n'-1,n}^2(u) + F_{n',n-1}^2(u)] - \frac{sp_z c + s' \eta' p_n' c}{\sqrt{\epsilon^2 - m^2 c^4}} [F_{n',n}^2(u) - F_{n'-1,n-1}^2(u)]. \end{aligned} \quad (6.15)$$

We change the variable q_y to u and perform the integration as follows,

$$\begin{aligned} \int dq_x dq_y &= m\omega_B \int \frac{dq_x du}{\sqrt{2m\omega_B u - q_x^2}} \\ &= m\omega_B \pi \int du \end{aligned} \quad (6.16)$$

Finally, the particle scattering rate becomes,

$$I_{fi} = \frac{n_i}{2} \int du (n_f(p) - n_f(p')) \left[\frac{1}{3(u + \frac{\xi}{3})(u + \xi)} - \frac{v_f^2}{6u(u + \frac{\xi}{3})} \right] \mathcal{F}. \quad (6.17)$$

-
- [1] B. P. Abbott *et al.* [LIGO Scientific and Virgo], Phys. Rev. Lett. **119** (2017) no.16, 161101 doi:10.1103/PhysRevLett.119.161101 [arXiv:1710.05832 [gr-qc]].
- [2] B. P. Abbott *et al.* [LIGO Scientific, Virgo, Fermi-GBM and INTEGRAL], Astrophys. J. Lett. **848** (2017) no.2, L13 doi:10.3847/2041-8213/aa920c [arXiv:1710.05834 [astro-ph.HE]].
- [3] B. P. Abbott *et al.* [LIGO Scientific, Virgo, Fermi GBM, INTEGRAL, IceCube, AstroSat Cadmium Zinc Telluride Imager Team, IPN, Insight-Hxmt, ANTARES, Swift, AGILE Team, 1M2H Team, Dark Energy Camera GW-EM, DES, DLT40, GRAWITA, Fermi-LAT, ATCA, ASKAP, Las Cumbres Observatory Group, OzGrav, DWF (Deeper Wider Faster Program), AST3, CAASTRO, VINROUGE, MASTER, J-GEM, GROWTH, JAGWAR, CaltechNRAO, TTU-NRAO, NuSTAR, Pan-STARRS, MAXI Team, TZAC Consortium, KU, Nordic Optical Telescope, ePESSTO, GROND, Texas Tech University, SALT Group, TOROS, BOOTES, MWA, CALET, IKI-GW Follow-up, H.E.S.S., LOFAR, LWA, HAWC, Pierre Auger, ALMA, Euro VLBI Team, Pi of Sky, Chandra Team at McGill University, DFN, ATLAS Telescopes, High Time Resolution Universe Survey, RIMAS, RATIR and SKA South Africa/MeerKAT], Astrophys. J. Lett. **848** (2017) no.2, L12 doi:10.3847/2041-8213/aa91c9 [arXiv:1710.05833 [astro-ph.HE]].
- [4] T. Kawamura, B. Giacomazzo, W. Kastaun, R. Ciolfi, A. Endrizzi, L. Baiotti and R. Perna, Phys. Rev. D **94** (2016) no.6, 064012 doi:10.1103/PhysRevD.94.064012 [arXiv:1607.01791 [astro-ph.HE]].
- [5] V. Paschalidis, Class. Quant. Grav. **34** (2017) no.8, 084002 doi:10.1088/1361-6382/aa61ce [arXiv:1611.01519 [astro-ph.HE]].
- [6] M. Ruiz, R. N. Lang, V. Paschalidis and S. L. Shapiro, Astrophys. J. Lett. **824** (2016) no.1, L6 doi:10.3847/2041-8205/824/1/L6 [arXiv:1604.02455 [astro-ph.HE]].
- [7] C. Palenzuela, L. Lehner, M. Ponce, S. L. Liebling, M. Anderson, D. Neilsen and P. Motl, Phys. Rev. Lett. **111** (2013) no.6, 061105 doi:10.1103/PhysRevLett.111.061105 [arXiv:1301.7074 [gr-qc]].
- [8] L. Baiotti and L. Rezzolla, Rept. Prog. Phys. **80** (2017) no.9, 096901 doi:10.1088/1361-6633/aa67bb [arXiv:1607.03540 [gr-qc]].
- [9] K. Kiuchi, Y. Sekiguchi, K. Kyutoku, M. Shibata, K. Taniguchi and T. Wada, Phys. Rev. D **92** (2015) no.6, 064034 doi:10.1103/PhysRevD.92.064034 [arXiv:1506.06811 [astro-ph.HE]].
- [10] K. Kiuchi, K. Kyutoku, Y. Sekiguchi and M. Shibata, Phys. Rev. D **97** (2018) no.12, 124039 doi:10.1103/PhysRevD.97.124039 [arXiv:1710.01311 [astro-ph.HE]].
- [11] M. Anderson, E. W. Hirschmann, L. Lehner, S. L. Liebling, P. M. Motl, D. Neilsen, C. Palenzuela and J. E. Tohline, Phys. Rev. Lett. **100** (2008), 191101 doi:10.1103/PhysRevLett.100.191101 [arXiv:0801.4387 [gr-qc]].
- [12] Y. T. Liu, S. L. Shapiro, Z. B. Etienne and K. Taniguchi, Phys. Rev. D **78** (2008), 024012 doi:10.1103/PhysRevD.78.024012 [arXiv:0803.4193 [astro-ph]].
- [13] K. Dionysopoulou, D. Alic, C. Palenzuela, L. Rezzolla and B. Giacomazzo, Phys. Rev. D **88** (2013), 044020 doi:10.1103/PhysRevD.88.044020 [arXiv:1208.3487 [gr-qc]].
- [14] K. Dionysopoulou, D. Alic and L. Rezzolla, Phys. Rev. D **92** (2015) no.8, 084064 doi:10.1103/PhysRevD.92.084064 [arXiv:1502.02021 [gr-qc]].
- [15] M. Ruiz, S. L. Shapiro and A. Tsokaros, Phys. Rev. D **97** (2018) no.2, 021501 doi:10.1103/PhysRevD.97.021501 [arXiv:1711.00473 [astro-ph.HE]].
- [16] C. Palenzuela, L. Lehner, O. Reula and L. Rezzolla, Mon. Not. Roy. Astron. Soc. **394** (2009), 1727-1740 doi:10.1111/j.1365-2966.2009.14454.x [arXiv:0810.1838 [astro-ph]].
- [17] C. Palenzuela, L. Lehner, S. L. Liebling, M. Ponce, M. Anderson, D. Neilsen and P. Motl, Phys. Rev. D **88** (2013) no.4, 043011 doi:10.1103/PhysRevD.88.043011 [arXiv:1307.7372 [gr-qc]].

- [18] A. Harutyunyan, A. Nathanail, L. Rezzolla and A. Sedrakian, *Eur. Phys. J. A* **54** (2018) no.11, 191 doi:10.1140/epja/i2018-12624-1 [arXiv:1803.09215 [astro-ph.HE]].
- [19] M. G. Alford, L. Bovard, M. Hanauske, L. Rezzolla and K. Schwenzer, *Phys. Rev. Lett.* **120** (2018) no.4, 041101 doi:10.1103/PhysRevLett.120.041101 [arXiv:1707.09475 [gr-qc]].
- [20] D. G. Yakovlev and V. A. Urpin, *Sov. Astron.* **3** (1980) 24.
- [21] L. Hernquist, *Astrophys. J.* **56** (1984) 325.
- [22] A. Y. Potekhin, *Astron. Astrophys.* **306** (1996), 999-1010 [arXiv:astro-ph/9603133 [astro-ph]].
- [23] A. Y. Potekhin and D. G. Yakovlev, *Astron. Astrophys.* **314** (1996), 341 [arXiv:astro-ph/9604130 [astro-ph]].
- [24] A. A. Abrikosov, *Soviet Physics JETP* **18** (1964) 1399–1404.
- [25] W. B. Hubbard, *Astrophys. J.* **146** (1966) 858.
- [26] M. Lampe, *Phys. Rev.* **170** (1968), 306-319 doi:10.1103/PhysRev.170.306
- [27] E. Flowers and N. Itoh, *Astrophys. J* **206** (1976) 218-242. doi:10.1086/154375.
- [28] A. Schmitt and P. Shternin, *Astrophys. Space Sci. Libr.* **457** (2018), 455-574 doi:10.1007/978-3-319-97616-7_9 [arXiv:1711.06520 [astro-ph.HE]].
- [29] R. Nandkumar and C. J. Pethick, *Mon. Not. Roy. Astron. Soc.* **209** (1984) no.4, 511-524 doi:10.1093/mnras/209.3.511.
- [30] E. Braaten and R. D. Pisarski, *Nucl. Phys. B* **337** (1990), 569-634 doi:10.1016/0550-3213(90)90508-B
- [31] E. Braaten and R. D. Pisarski, *Nucl. Phys. B* **339** (1990), 310-324 doi:10.1016/0550-3213(90)90351-D
- [32] T. Altherr and U. Kraemmer, *Astropart. Phys.* **1** (1992), 133-158 doi:10.1016/0927-6505(92)90014-Q
- [33] M. Le Bellac and C. Manuel, *Phys. Rev. D* **55** (1997), 3215-3218 doi:10.1103/PhysRevD.55.3215 [arXiv:hep-ph/9609369 [hep-ph]].
- [34] C. Manuel, *Phys. Rev. D* **62** (2000), 076009 doi:10.1103/PhysRevD.62.076009 [arXiv:hep-ph/0005040 [hep-ph]].
- [35] H. Heiselberg and C. J. Pethick, *Phys. Rev. D* **48** (1993), 2916-2928 doi:10.1103/PhysRevD.48.2916
- [36] S. Sarkar and A. K. Dutt-Mazumder, *Phys. Rev. D* **82** (2010), 056003 doi:10.1103/PhysRevD.82.056003 [arXiv:1005.1541 [hep-ph]].
- [37] S. Sarkar and A. K. Dutt-Mazumder, *Phys. Rev. D* **84** (2011), 096009 doi:10.1103/PhysRevD.84.096009 [arXiv:1105.5273 [hep-ph]].
- [38] S. Sarkar and A. K. Dutt-Mazumder, *Phys. Rev. D* **87** (2013) no.7, 076003 doi:10.1103/PhysRevD.87.076003 [arXiv:1209.5153 [nucl-th]].
- [39] S. P. Adhya, P. K. Roy and A. K. Dutt-Mazumder, *J. Phys. G* **41** (2014), 025201 doi:10.1088/0954-3899/41/2/025201 [arXiv:1303.6126 [hep-ph]].
- [40] S. P. Adhya, P. K. Roy and A. K. Dutt-Mazumder, *Phys. Rev. D* **86** (2012), 034012 doi:10.1103/PhysRevD.86.034012 [arXiv:1204.2684 [hep-ph]].
- [41] A. Harutyunyan and A. Sedrakian, *Phys. Rev. C* **94** (2016) no.2, 025805 doi:10.1103/PhysRevC.94.025805 [arXiv:1605.07612 [astro-ph.HE]].
- [42] A. I. Akhiezer and V. B. Berestetskii, *Quantum Electrodynamics*, Interscience Publishers, (1965)
- [43] L. P. Pitaevskii and E.M. Lifshitz, *Physical Kinetics*. Butterworth-Heinemann, (2012).
- [44] N. Chamel and P. Haensel, *Living Rev. Rel.* **11** (2008), 10 doi:10.12942/lrr-2008-10 [arXiv:0812.3955 [astro-ph]].
- [45] D. G. Yakovlev, *Astrophys. and Space Science* **98** (1984), 37-59 doi:10.1007/BF00651950.
- [46] A. Harutyunyan, GSI-2019-00453.
- [47] L. Rezzolla and O. Zanotti, *Relativistic Hydrodynamics*. Oxford University Press, Oxford, UK, 2013. 10.1093/acprof:oso/9780198528906.001.0001.
- [48] G. Baym, C. Pethick and P. Sutherland, *Astrophys. J.* **170** (1971), 299-317 doi:10.1086/151216
- [49] R. Nandi and D. Bandyopadhyay, *J. Phys. Conf. Ser.* **312** (2011), 042016 doi:10.1088/1742-6596/312/4/042016 [arXiv:1012.5973 [astro-ph.HE]].
- [50] A. Das, S. Sarkar and S. P. Adhya (in preparation).